TD-03-020
May 2003

Fermi National Accelerator Laboratory
Technical Division / Development & Test Dept.
PO Box 500 MS 316
Batavia, IL 60510
FAX: 630-840-2383

Test Report of Thermal Shock Experiment on Small Nb_3Sn Racetrack Magnet

L. Imbasciati, P. Bauer, G. Ambrosio, M. Lamm, A.V. Zlobin
Fermilab – Technical Division / Development and Test Department
S. Caspi, L. Chiesa, D. Dietrich, A. Lietzke, S. Gourlay,
LBNL - AFRD Division / High Field Magnet Group

Abstract:

In the R&D effort towards a post-LHC hadron collider, Fermilab and LBNL are developing 10-15 T Nb_3Sn dipole magnets using several design approaches. These magnets use Nb_3Sn superconductor technology. Nb_3Sn is a brittle material and it is yet not well known to what extent it may be affected by thermo-mechanical stress/strain during a magnet quench, inducing temperatures above 300 K at the hot spot. Rapid thermal expansion of conductor and large temperature gradients during a magnet quench can result in permanent critical current degradation and thus affect the performance of a magnet. In designing efficient quench protection systems, it is necessary to define the maximum temperatures that can be attained in the coils during a quench. Although critical current versus strain data are well known for Nb_3Sn, little is known how these limitations apply to the case of a cable thermally expanding in a magnet during a quench. To measure the effect of the thermo-mechanical shock exerted on the coil during a quench, an experiment was performed on a small magnet at LBNL. The experiment description and results are presented in this note.

1.0 Introduction

During quenches in superconducting magnets, parts of the coils can reach very high temperatures if the proper protection measures are not taken. Even in the case of actively protected magnets, it has to be determined which level of temperatures and voltages the magnet can sustain without degradation. An upper temperature limit is given by the melting point of the soldering (~500 K), since the quench might start near the conductor joints. For impregnated coils, a second limit could be the glass transition point of the insulation, which occurs at about 430 K for epoxy resins. At this temperature, the epoxy becomes soft and, even if the transition is reversible, the changes in its electrical properties increase the probability of a short circuit. In the case of magnets using Nb_3Sn superconductor, an additional complexity is introduced because of the brittleness of Nb_3Sn, which can be permanently degraded in its current carrying capability, under the effect of stress. Simulations of the quench process for Fermilab's Nb_3Sn magnets, in the context of a recent study of a Very Large Hadron Collider (VLHC) [1], have revealed the need to establish a maximum acceptable temperature that strongly affect the size/cost of the active quench protection system.

There are various possible ways to estimate the effect of magnet quenching and the ensuing thermo-mechanical stress on the critical current of brittle Nb_3Sn conductor. One way is to use finite element model calculations of the stresses/strains induced in the conductor during a magnet quench (including a simulation of the magnet quench process itself), which can be related to the well-known critical-current versus strain characteristics of Nb_3Sn strands. Efforts to obtain a result from calculations with this approach are underway at Fermilab and LBNL. A second way is to perform experiments that reproduce as realistically as possible the thermo-mechanical conditions in a coil during quench. A first experiment was performed on cables, within a collaboration FNAL-NHMFL. The results of this experiment were published in [2], [3]. Here we describe a new experiment recently performed on a LBNL small magnet, within the collaboration FNAL-LBNL.

1.1 Concept of the Experiment

The coils are instrumented with a spot heater each, and two voltage taps across the spot heater section. The magnet is trained until a quench plateau is reached.

At a current below the quench current, a quench is started with one spot heater. The quench is left propagating along the cable instead of switching off the current immediately, using a pre-defined delay. The current in the normal-conducting matrix allows a well-defined amount of heating of the cable. The normal conducting zone propagates in the coil, with a temperature profile that goes from the peak temperature of the starting point, to the bath temperature in other regions of the coils and in the supporting structure. The temperature gradients that are created in this fast process can induce the sought thermo-mechanical stress.

Repeated measurements of the quench current of the coils, after each excursion to high temperatures, allow assessing the critical current degradation as a function of the peak temperature during a quench.

1.2 General features of the LBNL Subscale Magnet Program

The Subscale Magnet Program [4], [5] was launched at LBNL with the aim of addressing R&D issues in a fast and cost effective way. In fact, building a small magnet (about 1/3 scale with respect to a short model magnet) requires a much lower amount of resources than a real scale, or even a short model accelerator magnet. In addition, the magnet structure is completely reusable. A sub-scale mechanical model was first used to test the pressurized bladder technology for applying pre-stress to the structure [6], a technology that was then successfully used for short model magnets (for example RD-3 magnet series). Each coil is made of ~20-meter long sub-sized cable (8 mm wide, 1.3 mm thick), and tests can be performed in a small cryostat, without the use of large background field magnets. Therefore, the Subscale Magnets are an effective way to test state-of-the-art conductor.

The general LBNL Subscale Magnet parameters are:

- Field range: 8 – 12 tesla
- Maximum current: 8 – 10 kA
- Magnet inductance: 0.2 – 0.4 mH
- Stored energy: < 20 kJ
- Two “double-pancake” racetrack coils (i.e. each coil is wound in two layers without interlayer splice)
- Conductor per coil: ~ 5 kg

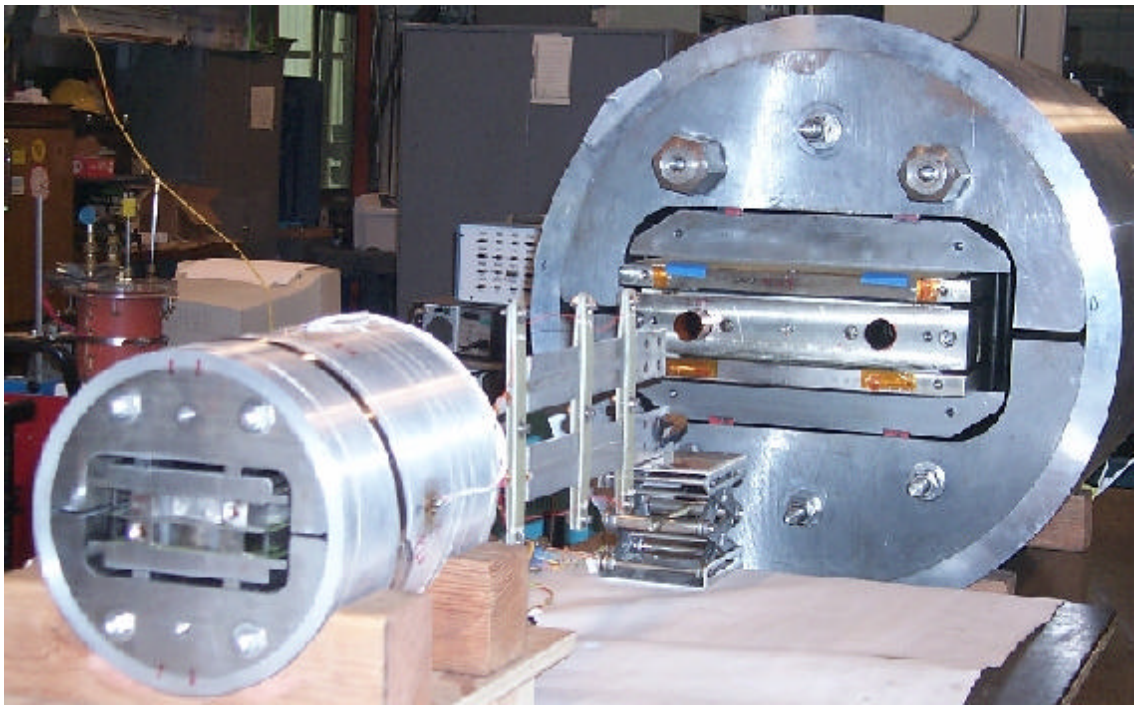

Figure 1: RD3 magnet (in the back), and Subscale Magnet (in the front) (LBNL Supercon Group).

1.2.a Field distribution

The magnet design consists of two "double-pancake racetrack" coils, connected in a common coil configuration (i.e. the current in one coil flows in opposite directions with respect to the current in the other coil). As can be seen in Figure 1, the magnet has no bore, and the coils are separated by a small gap. The field distribution, computed for the baseline configuration, is shown in Figure 2 and in Figure 3 [7]. The field pattern is typical of racetrack coils in the common coil configuration: the field is maximum along the inner edge of the first layer and close to zero towards the external side of the second layer.

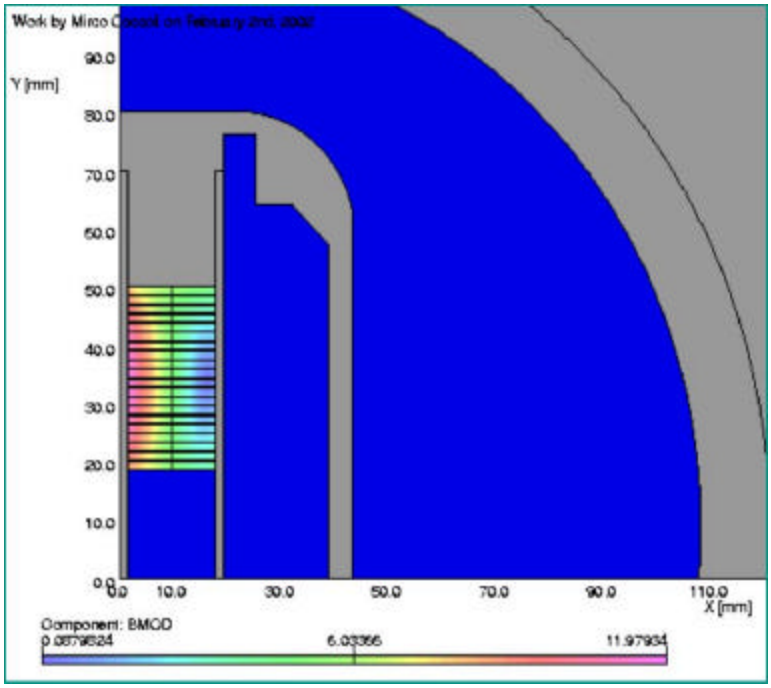

Figure 2: Magnetic field intensity (tesla) in one quadrant of the cross section of the LBNL Subscale Magnet (calculated for SM01at 9.9 kA).

The 3D analysis (Figure 3) showed that the peak field occurs in the straight section thanks to the effect of the iron of the yoke, the island, and the pads, in the shape as shown in Figure 3. The peak field intensity in the ends is about 10 % less than the peak field in the straight section.

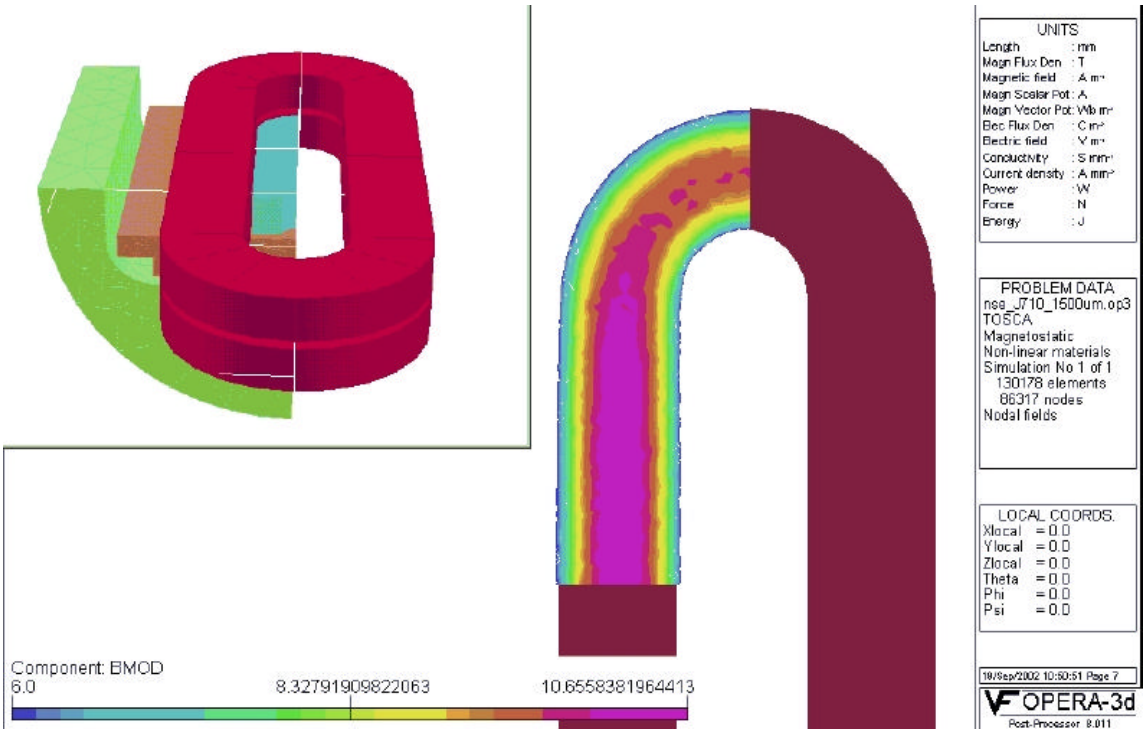

Figure 3: Magnetic field intensity (tesla) in one quadrant of the LBNL Subscale Magnet, calculated for SM03 at 8864 A, with 3 mm gap between the coils, using the model shown in the left corner (work performed by M. Coccoli)

1.2.b Instrumentation and Test

The Subscale Magnets are usually equipped with a very basic instrumentation, consisting of a couple of voltage taps across each splice, a temperature sensor for each module close to the splices, and some resistive strain gauges on the shell mid-plane. There are no quench protection heaters, since the protection system relies on energy extraction through an external dump resistor of ~50 mΩ. Additional instrumentation is added when it is needed in order to study specific technological issues.

The Subscale Magnets are tested at the LBNL-Supercon test facility using a small cryostat**,** which does not require the use of a refrigerator. Liquid helium is transferred from dewars.

There are two different data acquisition systems. One data system is used for registering the voltage signals during quench, with an acquisition rate of 0.2-1 ms, which is inversely proportional to the quench duration (having a fixed data file size). Another acquisition system is used to register fast events, such as magnetic flux changes due to conductor motion. The acquisition rate is of the order of 10 μs.

2.0 Test proposal and specifications for thermal shock test

As described in [3], the quench tests on cables, such as at the NHMFL test facility, lacked some mechanical features characteristic of an accelerator magnet. In particular, the mechanical support in the cross-section of the cable sample holder was weak. The use of LBNL small coils allows a continuation and an improvement of the quench tests program. In fact, the facility at LBNL allowed the use of state-of-the-art Nb_3Sn conductor, in a mechanical environment similar to that of an accelerator magnet. In order to clearly see a degradation of the critical current, it is necessary to operate the magnet close to the short sample limit, or to reach a reproducible quench current (flat plateau). The LBNL Subscale Magnets, using standard cable and state-of-the-art Nb_3Sn strands, have routinely achieved the predicted short sample current in the past. . In addition to reasons mentioned above, there were other factors, such as fabrication cost, helium consumption, and time required for measurement preparation, which made it more advantageous to perform the quench test on a Subscale Magnet than on an accelerator magnet model. Therefore, the LBNL small magnet program was ideal for the continuation of the experiments for the investigation of the thermo-mechanical effects of the quench.

However, some details of the experiment set up had to be addressed in order to reach the conditions required to perform the test. In particular, previous testing of Subscale Magnets has shown that the current decrease after a quench is very fast. Among the causes of the fast current decay are high quench propagation velocities, especially when the quench occurs very close to the short sample limit, a small inductance, and quench-back induced by the current decay.

To understand the quench process in the Subscale Magnets, we looked at previous quench studies, on one of these magnets, SM01-a [8]. In particular we compared the quench process during two events that occurred during the test of SM01-a. One is a "spontaneous" quench, occurred during training of SM01-a, and the second is a spot heater induced quench, at a current just below the short sample limit. Figure 4 shows the voltage imbalance between the two coils of the magnet.

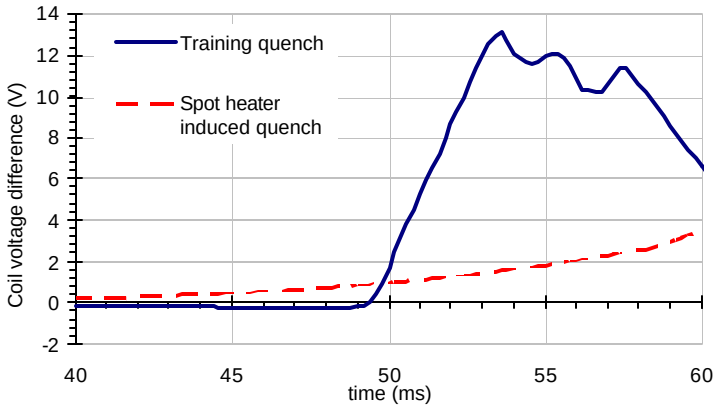

Figure 4: Voltage difference between the two coils of the magnet SM01-a, after a quench occurred during training and after a spot heater induced quench. The voltage rise during the training quench is much steeper than the voltage rise after the spot heater induced quench.

We can see that during the "training" quench, the resistive voltage rose very fast reaching a dV/dt of 1000 V/s in ~1 ms. A few ms after the quench in the first coil, the voltage imbalance dropped, because the resistance in the second coil started to rise, due to the so-called quench-back. The voltage rise, during the quench induced by the spot heater, was much slower than during the training quench, and the quench-back did not occur, during the 20 ms before the dump connection.

The rate of the voltage rise affects the current decay, as shown in Figure 5.

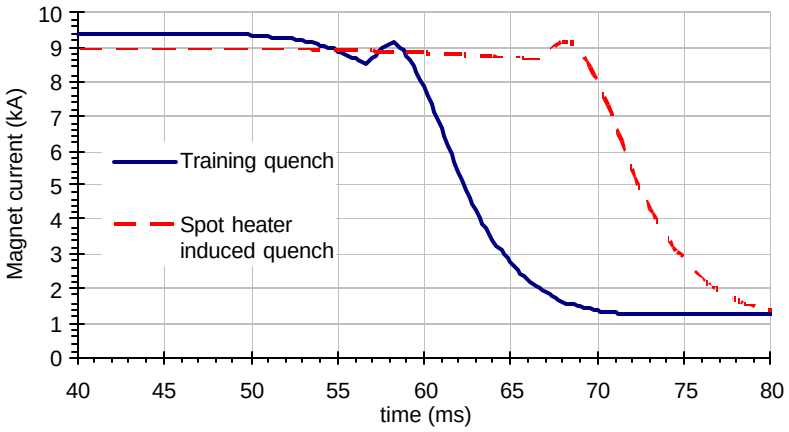

Figure 5: Current decays after a quench occurred during training and after the spot heater induced quench during the test of SM01-a.

The same figure shows that after the spot heater induced quench, the current decayed by about 300 A in 30 ms (total $\Delta I/\Delta t$ = 10 kA/s), while, after the spontaneous quench, the current decayed by ~800 A in 8 ms (total $\Delta I/\Delta t$ = 100 kA/s). The instantaneous rates of current decay are even higher (Figure 6).

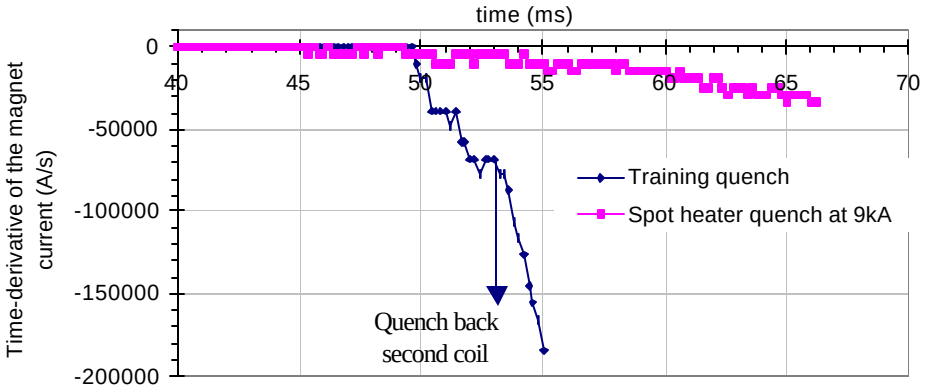

Figure 6: Time-derivative of the magnet current for training and spot heater induced quench of SM01-a.

To understand the quench-back phenomenon, we looked at the results of ramp rate studies (see Figure 18, and [10]), which indicate that ramp rates of 200 A/s, or higher, reduced the quench current to ~20% of the maximum current. On the other hand, Figure 6 shows that the quench-back did not occur, during the quench induced by the spot heater, until the current drop was higher than the 50000 A/s. Therefore, we can say that

the quench-back is not an immediate consequence of the current change, but there is a time delay, possibly due to a thermal response to eddy currents heating.

In order to reach temperatures of 300 K or higher, some modifications were implemented in the experiment set up, in order to keep the current at a high level for a longer time than in previous magnet tests. In fact, if the current remains almost constant even after the quench, the quench propagation can be limited to longitudinal and transverse propagation, the quench back can be avoided, and the temperature increases faster. During previous LBNL small magnet tests, the power supply was set in the voltage mode. In this mode, the current decreases according to the voltage rise. The current with the power supply in current mode, was not very stable. It turned out that having the power supply set in voltage mode, lead to faster current decays, and therefore worked almost like a passive protection system.

In fact, quench simulations showed that, in voltage mode, the current decay time is very sensitive to quench propagation velocities. Since there are uncertainties regarding the prediction of the quench propagation velocity, the quench was simulated several times using different values of these parameters. The results show that reaching temperatures of 300 K or higher might be difficult when quench velocities reach 80 m/s or higher (Figure 7).

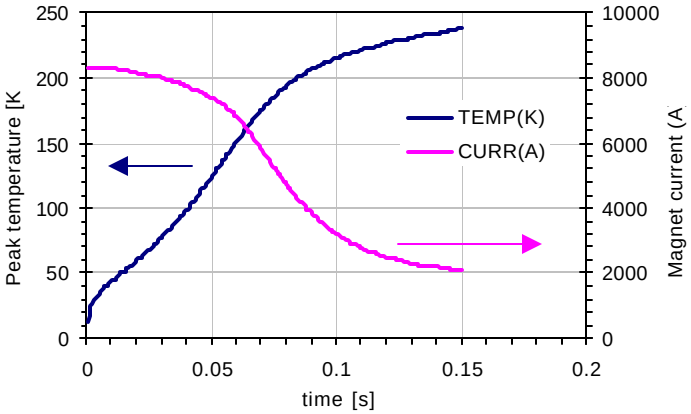

Figure 7: Quench process simulation with initial longitudinal quench velocity of ~80 m/s.

Therefore, the power supply was set in the current mode, in which the system supplies a constant current almost independently from the voltage of the magnet, up to 50-60 V. Non the less, in the first thermal cycle, even though the current generated by the power supply remained constant during quenches, part of the current flowed through another branch of the circuit. This additional circuit (consisting of a series of capacitors) was used to improve the stability of the current during the ramp. In the second thermal cycle, most of the capacitors were removed, in order to maintain high currents after the quench until the voltage limit was reached

2.1 Specifications for the thermal shock test

Nine coils were fabricated before the coil devoted to the thermal shock quench test (coil # 10, labeled as SC10). Four magnets have been assembled with these coils and tested. The thermal shock quench test was performed on Subscale Magnet # 5 (labeled as SM05), consisting of SC10 and SC01 (coil # 1). Several modifications were introduced in the coil and magnet fabrication, in order to perform the thermal shock experiment.

2.1.a Conductor characteristics

The cable for the Subscale Magnets is fabricated at LBNL-Supercon-AFRD, superconducting cable group. The baseline conductor, used for most of the coils, is a MJR conductor, produced by Oxford. The main cable and conductor parameters for the two coils of SM05 are listed in (Table 1). The relative reaction cycle is shown in (Figure 8). The cable insulation used is an epoxy impregnated S2-glass sleeve.

The cable used for the fabrication of Coil 10 came from spool number S-3-O-00817 (details in cable log-sheet in appendix). The main difference between this cable and the cable used for SC01, is the copper content in the strands. The conductor for SC10 has 60% copper content, while SC01 has only 50%. Therefore, even with the same J_{non-Cu}, the current capacity of the strands is lower for SC10 than for SC01. In addition, the reaction cycle chosen for SC10 (reacted together with SC07 and SC09) was shorter than the reaction cycle for SC01. Test results of this reaction cycle show a slightly lower critical current density in the non-copper area, and a RRR relatively high for this type of conductor. Conductors reacted with thermal cycles optimized for high J_C, can have RRR as low as five. The lower critical current in SC10 than in SC01 assured that the coil under investigation determined the magnet current limit. In addition, a high RRR will cause a lower voltage rise, thus improving the stability of the current before activation of the dump switch.

Conductor parameters	Coil 1	Coil 10
N of strands	20	20
Manifactor	OST	OST
Cu:SC	0.87	1.5
Cable width (mm)	8	7.84
Cable thickness (mm)	1.3	1.27
Strand diameter (mm)	0.7	0.672
Pitch angle (°)	15.9	15.9
Packing factor	0.83	0.83
J_C (A/mm2) @12T/4.2K	2265	1763
I_{SS} (A)*	10010	9101
B_{peak} (T) in the coil at I_{SS}	11.82	10.57
Cu RRR	41	54
Insulation (mm)	0.15	0.15

Table 1: Conductor parameters of Subscale Magnet 5 coils.
* Best performance of SM01 and SM05 respectively.

SC10 was heat-treated following the cycle indicated in Figure 8 by the continuous line, while SC01 heat treatment is indicated by the dashed line.

The critical current of two "witness" samples (two virgin strand samples reacted together with the coil) was measured. The results are reported in Table 2. The total field reported in the table is the sum of the background field and the self-field induced by the sample. The cable current is obtained by multiplying the strand current by the number of strands (20), without taking into account possible cable degradation.

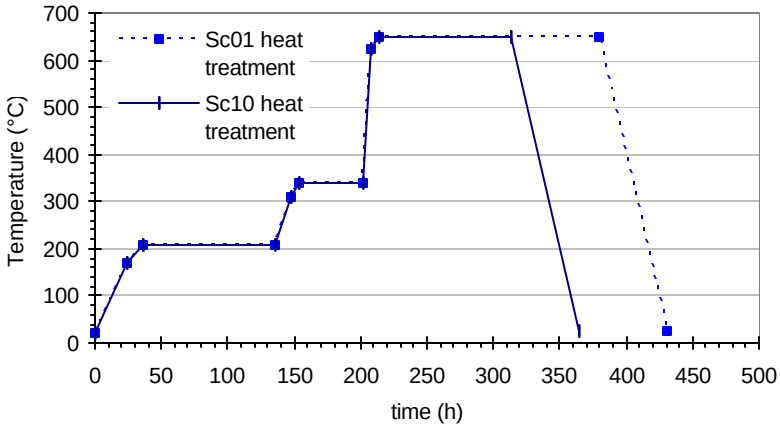

Figure 8: Heat treatment cycle for Sc01 and SC10.

Total Field (T)	Strand Sample L 26 Current (A)	Cable Current (kA)	Strand Sample L 35 Current (A)	Cable Current (kA)	Average Current (kA)
10.16	448	8.96			8.96
11.13	368	7.36	365	7.3	7.33
12.1	296	5.92	293	5.86	5.89

Table 2: I_c measurements of virgin strand samples, at 4.2 K, of the same strand type as used in cable 817, used for SC10.

The short sample current reported in Table 1 is the maximum current reached during the test of SM05 (see Figure 29). The peak field corresponding to this current, was computed using the load line in Figure 9. This load line was derived from an OPERA model of SM05, which takes into account that the actual size of the gap between the two coils of SM05 was 7.8 mm (slightly larger than the gap of previous magnets). The point of intersection between the load line and the strand critical current measurements is at 8.7 kA (8.34 T), slightly lower than the 9.1 kA maximum value reached during test.

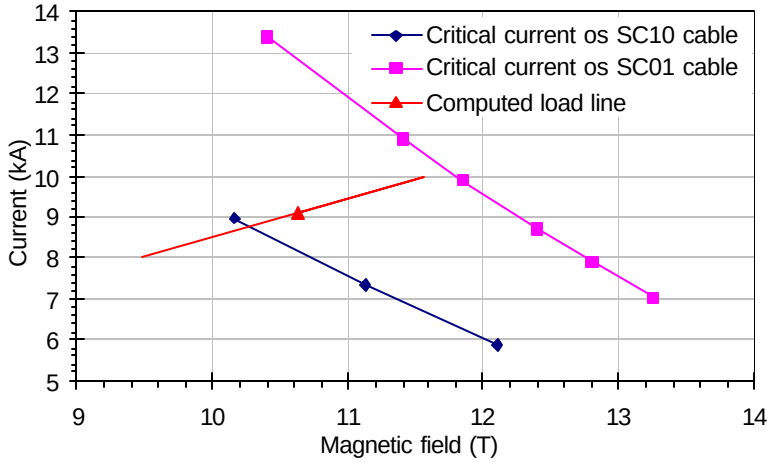

Figure 9: SM05 load line and strand critical currents for SC10 and SC01. The measured maximum current reached in SM05 test is indicated by the triangle.

2.1.b SC10 instrumentation

SC10 was instrumented with a spot heater in the high field region, voltage taps (VT) across the spot heater (SH), and a temperature sensor (TS) close to the spot heater. The spot heater and voltage tap positions over the inner layer of SC10 are indicated in Figure 10. The spot heater was put in a high field region (inner layer straight section), so that the effect of local degradation may result in a reduction of the magnet current.

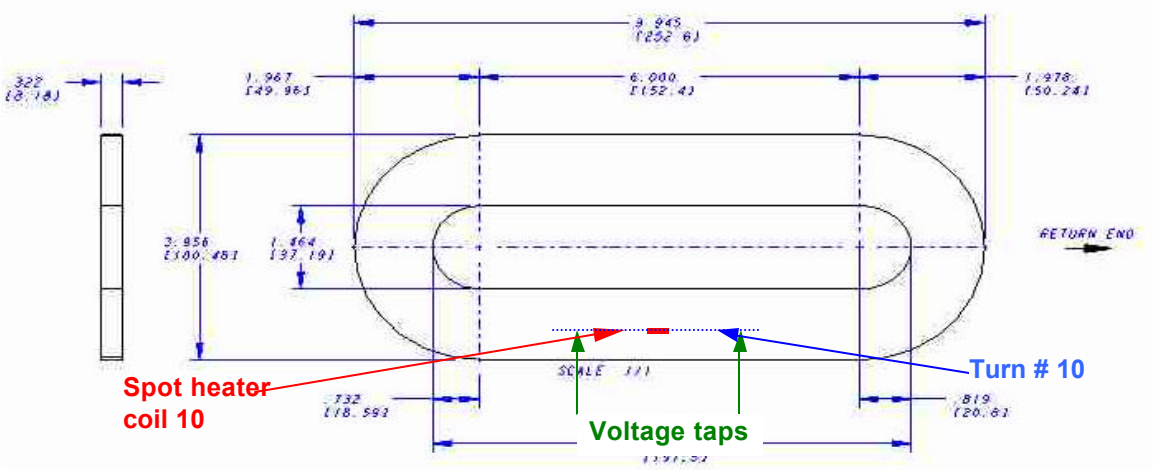

Figure 10: Coil geometry and instrumentation scheme (all dimensions in inches [mm]).

2.1.c Coil fabrication

After winding the first layer, with the standard tension of 40 lb over the cable, the coil turned out to be thinner than expected, and an extra turn was added, for a total of 21 turns per layer. The cable was found to be thinner because of a loose fit in the transition region. The total length of the cable used was 11.6 m for the first layer, and 11.2 m for the second. The coil instrumentation was installed during winding of the second layer (top layer, which corresponded to the inner layer of the magnet assembly).

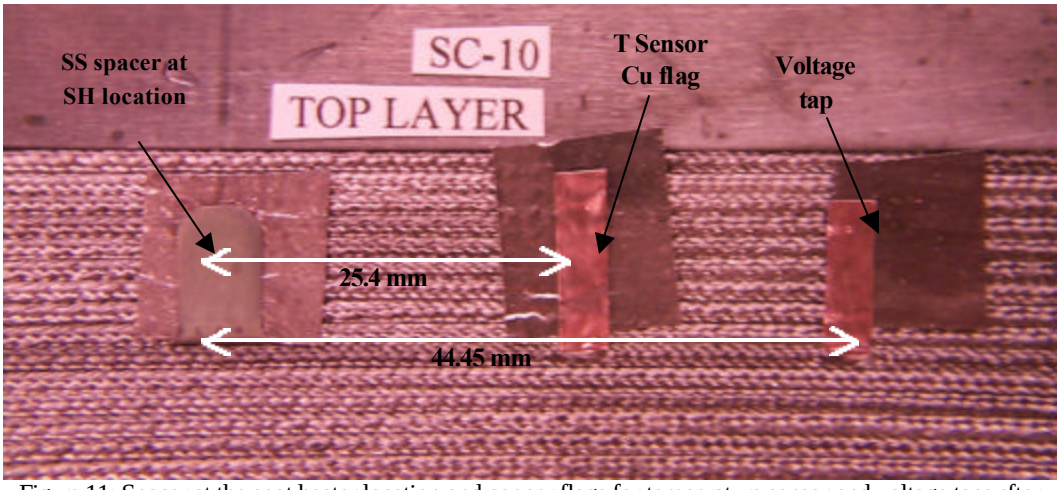

Figure 11: Spacer at the spot heater location and copper flags for temperature sensor and voltage taps after reaction.

A thin stainless steel spacer (0.005") was inserted between turns # 10 and # 11, where the spot heater was then inserted after the reaction. In addition, three thin copper strips were placed across the cable, on turn #10. Two of these strips were to be used as voltage taps, and one was used to attach the temperature sensor on it. The copper strips for the voltage taps are 88.9 mm apart (center to center), and the strip for the temperature sensor is 25.4 mm from the spot heater position (Figure 11).

The stainless steel spacer was removed after reaction to install the spot heater. The spot heater was fabricated according to a new design, to perform a four-wire measurement of the resistance of the spot heater. The two voltage tap leads, and the four stainless steel legs of the spot heater are connected to the circuit traced by photo edging on a Kapton foil ("trace"). The Kapton foil was trimmed to fit the coil dimension. Cuts were then made corresponding to the voltage tap locations, exposing the stainless steel pad, over which the copper flags were soldered. The spot heater was cut along three sides, bent, and inserted between turn 10 and 11. The insulation between the spot heater and turn 10 consists of 0.002"-thick Kapton (opaque side of the trace) plus the cable insulation. The insulation between the spot heater and turn 11 consists of 0.0045"-thick Kapton (glide side of the trace, 0.004", plus 0.0005" extra Kapton adhesive) plus the cable insulation. A cut allows the copper flag for the temperature sensor to come through the Kapton foil.

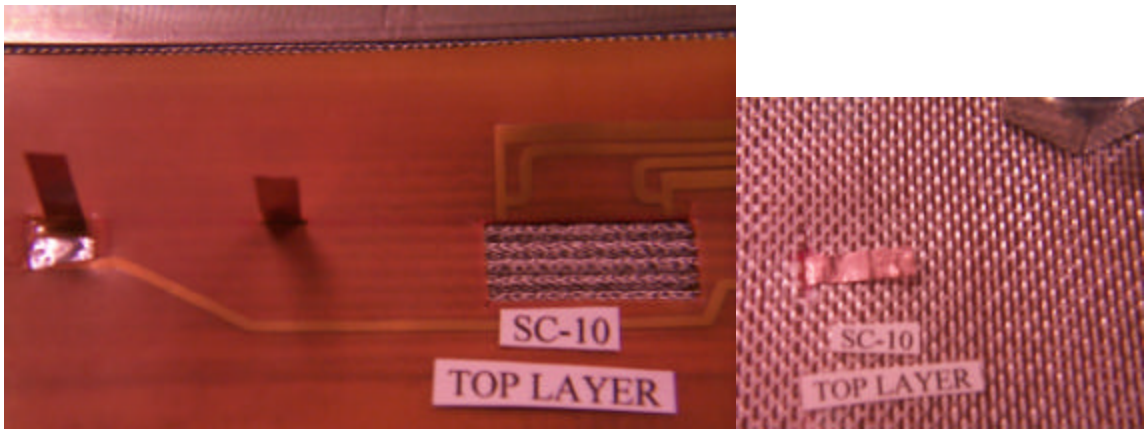

Figure 12: (a) The trace lies on the coil after reaction, before impregnation. The spot heater is inserted between two middle turns. The copper flags for temperature sensor and voltage taps emerge from the Kapton foil of the trace. (b) Copper flag for the temperature sensor protruding through the fiberglass mat on top of the coil.

After soldering the voltage taps to the trace, a 0.005" fiberglass mat, with a cut to provide passage of the copper flag carrying the temperature sensor, is laid on the coil. This layer of fiberglass is intended to help the epoxy impregnation of the entire coil. It prevents large air bubbles from being trapped, and prevents the formation of cracks after cool down [9]. After impregnation, the coil was inspected, and the impregnation was satisfactory on the top layer, but there were some small voids in the bottom layer/lead side. However, since previous coils have performed well despite the presence of similar voids, the coil was considered acceptable, even with a less than perfect impregnation.

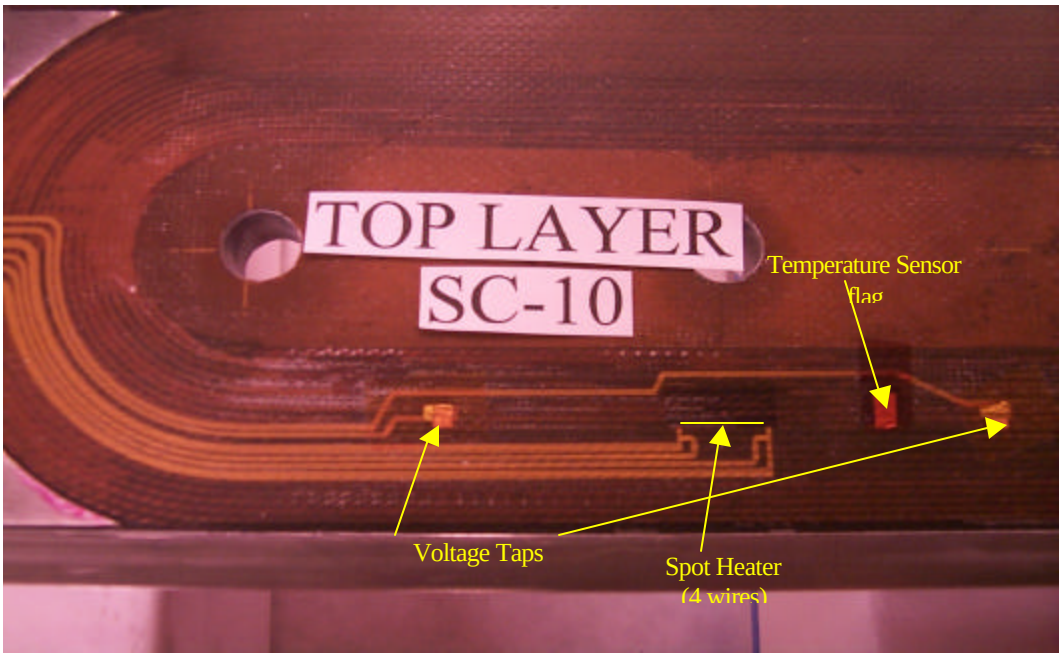

Figure 13: Top layer with instrumentation (inner layer in the magnet configuration), after impregnation.

Figure 14: Coil, bottom layer (outer layer in the magnet configuration), after impregantion.

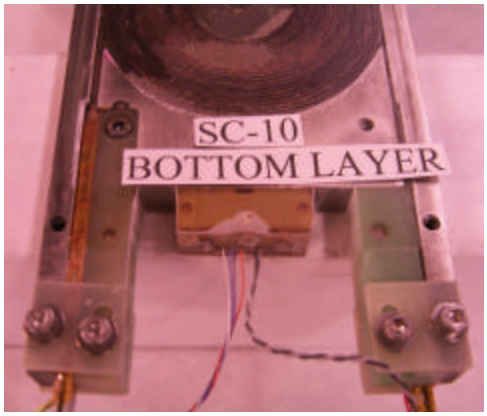

Figure 15: Impregnated coil: bottom layer (outer layer in the magnet configuration), lead end.

The temperature sensor (CERNOX type 1030-HD, package SD) was installed after the coil impregnation, and before magnet assembly. There is no bore between the two coils, but rather a spacer, made of several layers of insulation. Near the coils, are two

NEMA plates (0.1" thick). It was decided to place a split spacer between the two coils, so that the two layers would follow the coils when they separate from each other under Lorentz forces. The NEMA plate adjacent to SC10 has a hole and a groove 0.065" thick, in order to accommodate the temperature sensor and its wires. Two twisted pairs of wires connect the temperature sensor leads, in order to allow one to perform a four-wire measurement of the resistance. Stycast holds the wires in the place, and fills part of the channel, up to ~2 cm from the sensor. A small dab of Apiezon N was put on the contact area of the temperature sensor. The copper flag was trimmed to fit the sensor. A small amount of RTV was used to hold the sensor and to insulate the leads filling up the groove in the plate, from the sensor to the stycast.

After curing of the RTV, a small plug of fiberglass RTV-impregnated was used to fill the hole in the NEMA plate and to hold the sensor in position. This material was chosen for the plug in order to allow some pressure on the sensor and to improve the thermal contact. Thus, the use of a hard material that could damage the sensor was avoided.

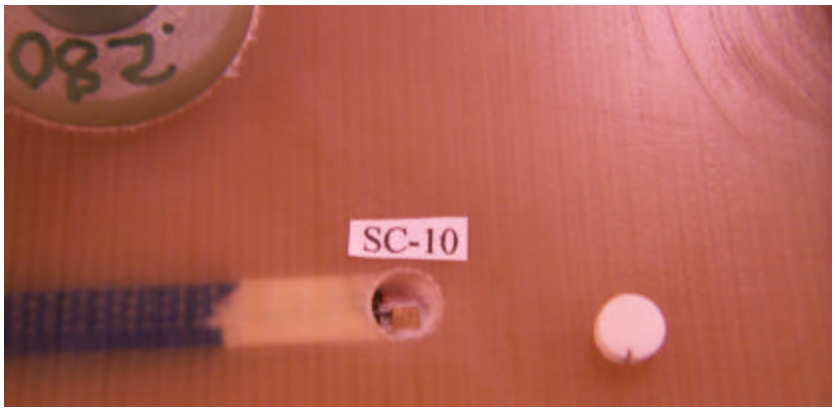

Figure 16: Temperature sensor under the NEMA layer with the groove for the wires, and a hole for the temperature sensor; a cap of RTV-impregnated fiberglass protects the sensor.

After the first thermal cycle, we carefully investigated the accuracy of the peak temperature reading in the coil after a quench. It was then noticed that LHe would be able to penetrate around the plug and come in close contact with the sensor, on the side and on the top of the sensor case, and at the lead joints. The additional cooling, due to the contact with LHe, is believed to be the cause of the reduced temperature reading of the sensor, with respect with the temperature derived from the resistance measured during the experiment.

2.1.d SM05 assembly

As described above, in order improve current stability after a quench, it was decided to increase the inductance as much as possible by opening the gap between the coils, thereby changing the position of the skins. All the stainless steel skins were replaced by NEMA skins, and placed between the two coils. The gap increase between the two coils decreases the mutual inductance of the two coils, thus helping to avoid quench-back of SC01.

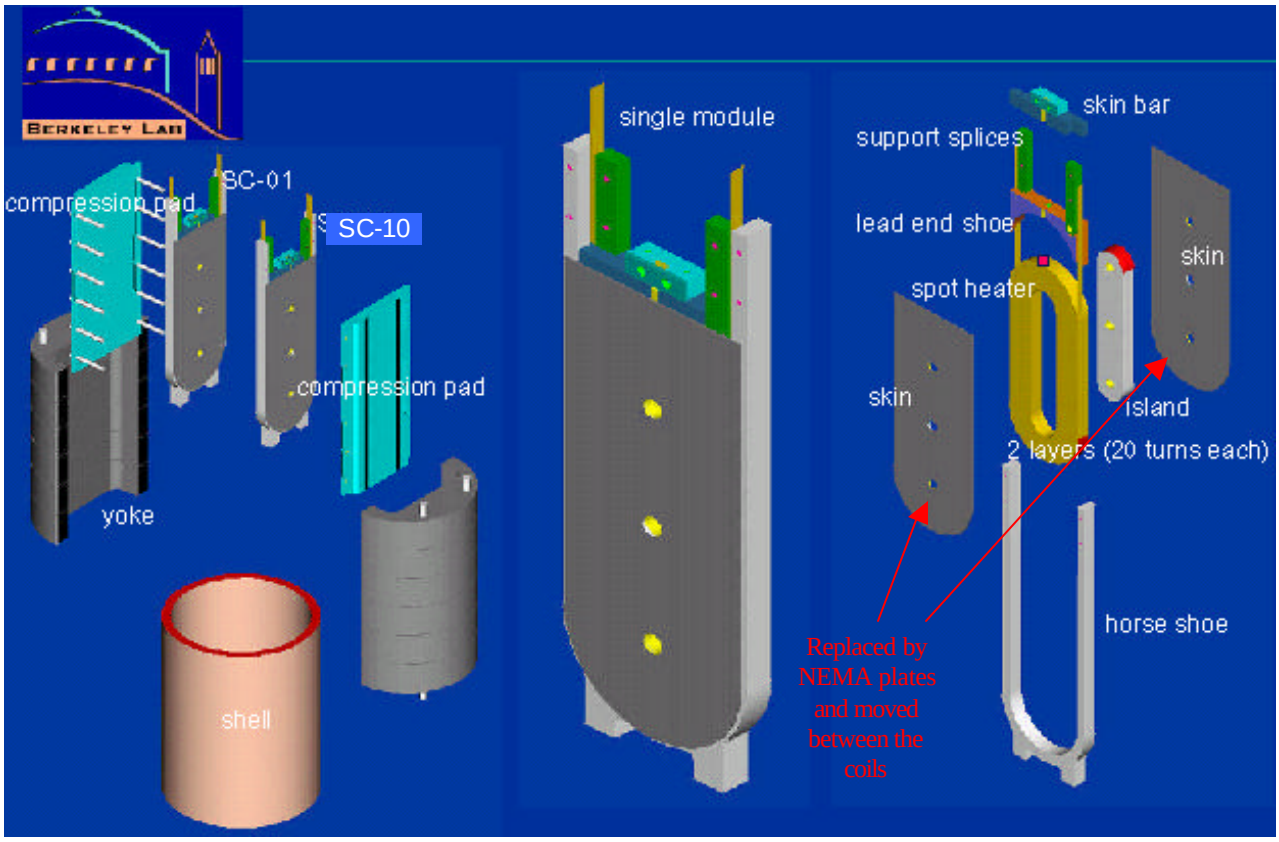

Figure 17: Magnet assembly.

Summarizing the main specifications for the assembly of SM05:

- Low pre-stress to allow separation, and therefore faster training (see training of SM01-a and SM01-b)
- Minimum size of the keys: 0.25'' (6.35 mm)
- Captured keys (to make sure they don't fall off when coils separate)
- From the dimension of the magnet components, the size of the central spacer was calculated to be 4.953 mm (see Table 3).

The following is the procedure, outlined for the SM05 assembly, used to keep the **vertically** oriented coil-pack in the shell structure, with a minimum coil pre-compression:

1. Set the coil on 0.25" keys.
2. Pump and purge the bladders 3 times to a minimum of 3000 psi (~20 MPa) to improve rigidity of the coil-pack.
3. Bring the bladder up to 1000-1100 psi (~7 MPa)
4. Install final keys (~ 0.25")
5. Depressurize bladders.
6. Bring bladder pressure up slowly until a key can be moved and record pressure (to have a good measurement of the final pressure).
7. Depressurize and disassemble bladders.

Structure Component	Thickness (mm)	Sum (mm)
PAD	16.510	
NEMA	0.127	
MYLAR	0.076	
NEMA	0.127	
SC10	16.764	
NEMA (TS)	2.540	36.144
SPACER (316)	**4.953**	
NEMA	0.127	
MYLAR	0.076	
NEMA	0.127	
SC01	16.764	
NEMA	0.127	
MYLAR	0.076	
NEMA	0.127	
PAD	16.510	33.934
Total Coil pack		70.079
Keys		6.350
Shell cavity		85.598

Table 3: Assembly of SM05 main parameters

2.1.e LBNL test facility setup for thermal shock test

The power supply was adjusted, in current mode, to provide a stable current. The system supplies a constant current almost independently from the voltage of the magnet, up to 50-60 V. Tests of the short-circuited power supply gave positive results. Unfortunately, during the first thermal cycle, we noticed that the response of the power supply connected with the small magnet was different than the room temperature measurements, and that the current drops quickly as for maintaining the voltage constant over the magnet. In fact, even though the current from the primary circuit of the power supply remains constant, part of the current flows through another branch of the circuit, which consists of a series of capacitors. This additional circuit path improves the stability of the current during the ramp. During the second thermal cycle, most of the capacitors were removed from the circuit, in order to keep the current high at the beginning of the quench (before the voltage limit is reached).

3.0 Program of the test

The following describes the program of the test, according to preceding calculations:

Before training
- Check instrumentation
- Check quench detection system through Manual Trip at I/Ic = 0.3 (3000A)
    - Check voltage signals
    - Current decay correspond to expected dump resistance and inductance

Training

After each quench, approximately
- Check voltage signals and quench location
- Check strain gages
- Current decay, MIIts and T_{peak} if quench starts at spot heater segment location

Ramp rate

-Observe and register temperature sensors behavior
-Find the maximum ramp rate that does not reduce the quench current $(dI/dt)_0$

Spot heater study

- Check quench detection system through Spot heater induced quench at I/Ic=0.3 (3000A)
    - Spot Heater Voltage and duration
    - Check voltage signals
    - Temperature sensor spot heater data
    - Current decay, MIIts and T_{peak} corresponds to calculations

Thermal shock Test

- Ramp magnet to about I/I_{ss} = 95%, at 8300 A, dump delay 40 ms, Spot heater induced quench
- Minimum Spot Heater Voltage to cause a quench and its discharge duration
- Check voltage signals
- Temperature sensor spot heater data
- Compare calculated predictions with real data for current decay, MIIts and T_{peak}
- Ramp to quench at $(dI/dt)_0$
- Check voltage signals and quench location

Spot heater induced quenches:
- Repeat for same magnet current, dump delay times to 60, 80, 100, 140, and 200 ms,
- Check voltage signals
- Temperature sensor spot heater data
- Compare calculated predictions and real data for current decay, MIIts and T_{peak}
- Check if voltage limit is reached in 60ms

After each spot heater event ramp to quench at $(dI/dt)_0$
- Check voltage signals and quench location

1) If T_{peak} does not reach 400 K, because voltage limit is reached early:
- Ramp magnet to about I/I_{ss} = 98%, at 8500 A, Spot heater induced quench, delay times to 140, and 200 ms
- Check voltage signals
- Temperature sensor data
- Current decay, MIIts and T_{peak} corresponds to calculations
- Training quench at $(dI/dt)_0$
- Check voltage signals for quench location and system OK

2) If T_{peak} still does not reach 400 K (because the quench is propagating too fast):
Repeat at I/I_{ss} = 85%, at 7500 A, Spot heater induced quench and again at 7000 A, and so on, reducing the magnet current by 1000 amps each time. The reduced current should reduce quench propagation velocities and increase total MIIts collected during the event.

4.0 Description of the Test

Before performing the thermal shock experiment, several tests were performed on the magnet according to the program of the test reported in the previous section. Among those, the residual resistivity ratio (RRR) of the coils was measured during cool down. The measured RRR of SC-01 was 41, and the RRR of SC-10 was 54.

4.1 Training and ramp rate study

The magnet training started by increasing the current up to the first quench, with a ramp rate of 15 A/s, and holding every thousand amps for a while, following the standard test procedure at LBNL. The very first quench occurred at low current due to low liquid helium level. The second quench occurred at 97.7% of the computed short sample current (SS). The magnet trained very fast, reaching 101.3 % of SS at the fifth quench. The highest current reached during the first thermal cycle was 8757 A (10.47 T), with a ramp rate of 15 A/s.

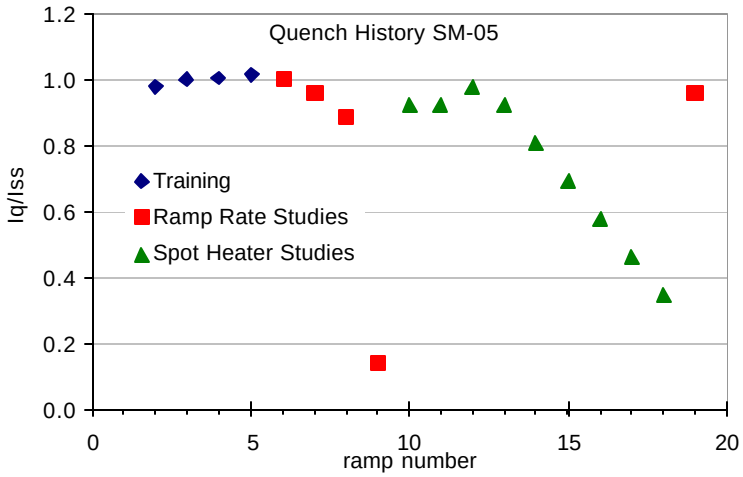

Figure 18: Quench history of SM05-first thermal cycle.

The brief training was expected, based on the previous experience at LBNL with small magnets. In fact, it was previously noticed that applying low pre-stress allows the coils to separate easily during magnet excitation [10]. It was chosen therefore, to apply a low pre-stress (see previous section 2.1.d) in order have a fast training, to allow for more time to the thermal shock test and to reach a clear quench current plateau.

During current ramps, the fast data logging system registered several events, similar to that shown in Figure 19. These events are interpreted as fast motion of conductor, or part of the coils. In fact, we see that the signals related to each coil have opposite signs, and therefore can be distinguished from power supply induced noise, and are also different from spikes due to flux motion in the superconductor, which last a fraction of ms (Figure 20). Some of the first training quenches were anticipated by such a fast motion signal. Successive quenches were not anticipated by fast motion (Figure 19-b), showing improvement in the training process.

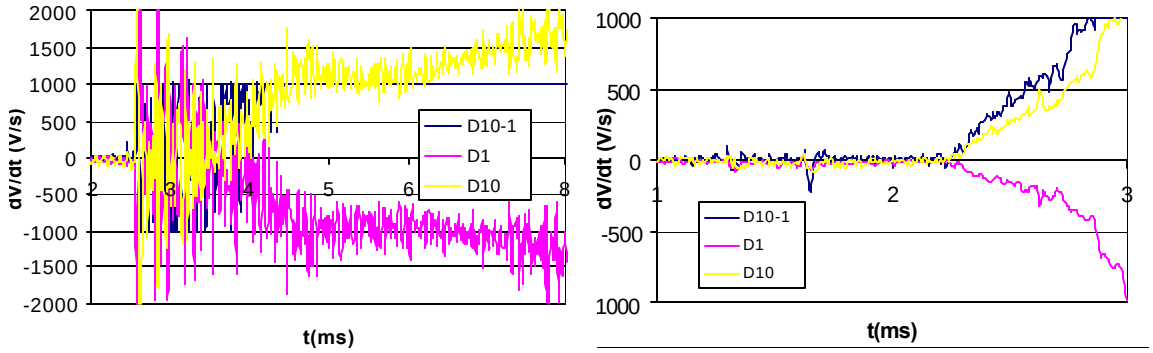

Figure 19: Fast motion event triggering quench # 2, and quench # 6 in SM05; the signals correspond to the voltage derivative over coil 10, coil 1 and the difference between the two (D10, D1, and D10-1)

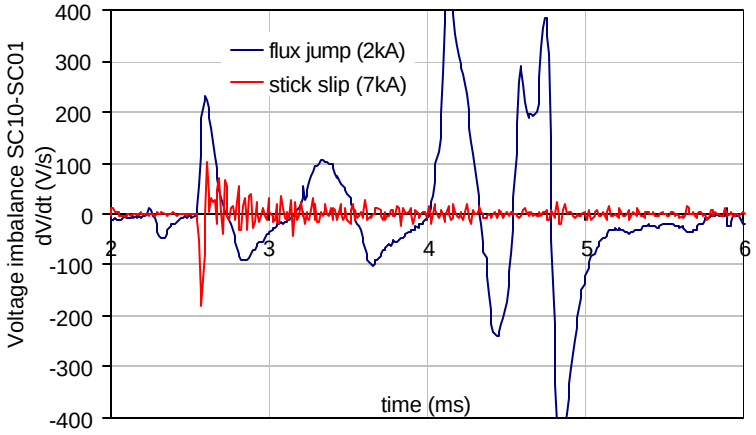

Figure 20: Fast motion ("stick slip") and flux jumps in quench #11 in SM05; the signals correspond to the voltage derivative of the difference between the coil 10 and coil 1.

After the training, the ramp rate dependence was measured (Figure 21). The ramp rate dependence of SM05 was similar to that of other small magnets. It is characterized by a quick drop of the quench current at ramp rates between 100 and 200 A/s [10].

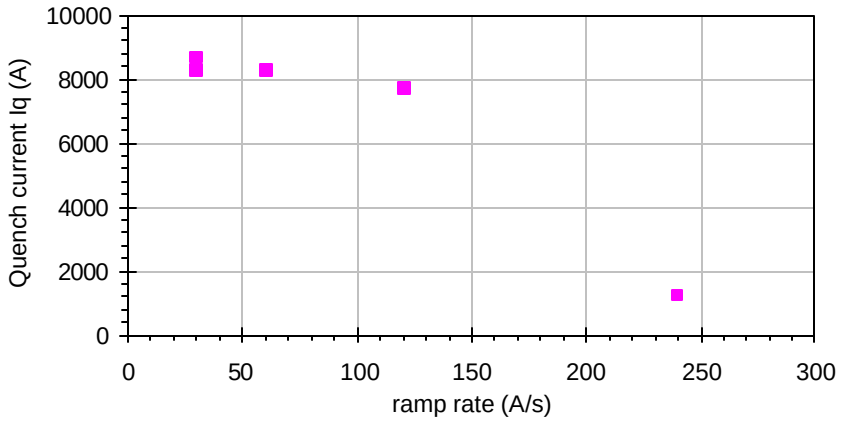

Figure 21: Ramp rate sensitivity of SM05.

4.2 Spot heater study

During the magnet test, spot heater studies were performed with the goal of finding the quench energy deposition needed to initiate a quench.

The spot heater was connected with an electronically controlled capacitor bank. The power supply electronic interface allows setting the charging rate and reading the actual voltage over the capacitors from a display. Since turning on and off the capacitor bank caused spikes that would induce a quench when the magnet was charged, the procedure for the quench energy tests was the following. Just before the ramp of the magnet current, the capacitor bank was turned on at a slow charging rate. At the end of the magnet current ramp, the voltage level in the capacitor was read, and the capacitor bank was fired.

At currents of 6 kA or below, the initial low voltage discharge would not induce a quench; when the voltage level was raised further, a quench was initiated. This procedure unfortunately prevents us from firing small energy amount corresponding to high currents in the magnet. In fact, at 6 kA, the voltage over the capacitor bank inducing a quench was 40 V (about 20 times the voltage over the spot heater itself). For currents of 7 kA or more, the magnet ramping took about five minutes or more, the capacitor charged up to a voltage over 40 V, and the capacitor discharge would induce immediately a quench. Table 4 reports the voltage over the capacitor bank during the quench test. The last row reports the voltage over the spot heater when the power supply was fired.

Magnet current (kA)	8.5	8	7	6	5	4	3
Voltage over bank capacitor (V)	46	40	41	32	28	24	20
				40	35	35	34
					39	41	41
					42	46	47
					69	52	49
						62	55
							58
							67
Quench voltage over PS (V)	46	40	41	40	69	62	67
Peak voltage over SH (V)	2.10	1.96	1.98	1.86	3.32	2.98	3.18

Table 4: Quench energy test: voltage over the bank capacitor and over the spot heater (V)

However, it was possible to calculate precisely the energy amount that induced the quench, by integrating the power deposited in the coil from the start of the capacitor discharge until the moment the quench started. Figure 22 shows the spot heater event at 5 kA. The results of the quench energy test are summarized in Table 4 and in Figure 23.

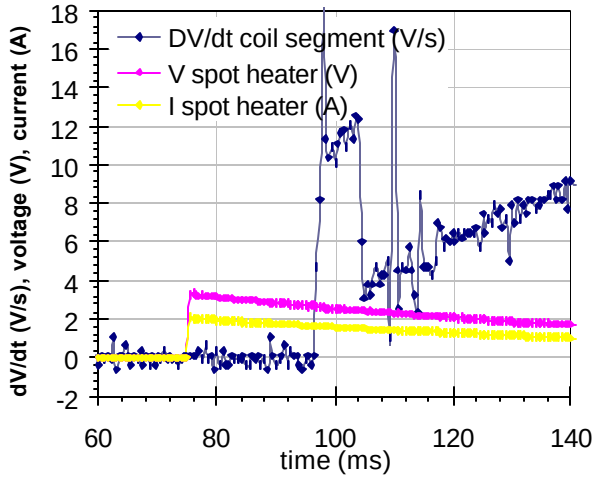

Figure 22: Spot heater event H07: voltage rise (V/s) of the spot heater segment after capacitor discharge and the voltage (V) and current (A) in the spot heater.

Ramp #	Magnet current (kA)	Energy to quench (mJ)	Time to quench (ms)	SH peak power (W)
H01	8.0	25	6	4.51
H02	8.0	19	7.6	2.65
H03	8.4	14	5.5	2.75
H04	8.0	17	8.5	2.32
H05	7.0	31	14.5	2.43
H06	6.0	58	39.5	2.14
H07	5.0	115	21	6.79
H08	4.0	145	39	5.48
H09	3.0	201	52	6.29

Table 5: Minimum quench energy data: energy and time to quench after heater firing, and peak power in the spot heater.

We have to notice that the energy amount reported here is not released solely in the strands, but it is distributed over the spot heater itself, the insulation of the spot heater (both sides), and the insulation of the cable. Therefore, the energy values reported here can be regarded as upper limits to the minimum quench energy. A thermal model could help estimating the energy released into the cable alone.

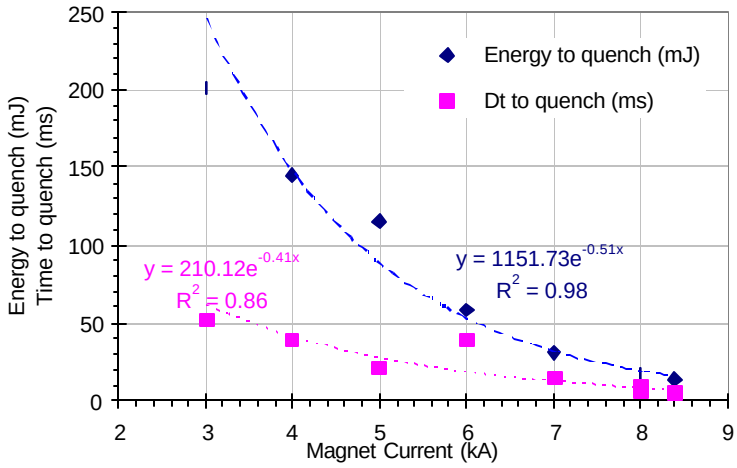

Figure 23: Minimum quench energy study: energy and time to reach quench after heater firing.

4.3 Thermal shock study

4.3.a Thermal cycle I

The thermal shock test began following the test plan, ramping the magnet to 8000 A (I/I_{ss} = 93%) at 30 A/s, setting a short dump delay time (10 ms), and inducing the quench with the spot heater. The short delay time was chosen in order to check the procedure, before causing damage to the magnet with a "thermal shock" type test.

In particular, we tried to find a minimum spot heater voltage to induce the quench, with minimum discharge duration. In fact, a more powerful capacitor discharge can enhance the normal zone propagation speed, increasing the resistive voltage growth, and therefore shortening the time before reaching the voltage limit of the power supply. As described in the previous section, we discovered that it was not possible to have such a low voltage, short pulse.

After the spot heater event, we checked the voltage signals, the data of the temperature sensor at the spot heater, and we compared the calculated predictions with the real quench integral and peak temperature data. In Figure 24, we see that after the quench, the current is not constant, even though the voltage over the magnet did not reach the power supply voltage limit. The current fell to 7.4 kA before the dump switch was activated.

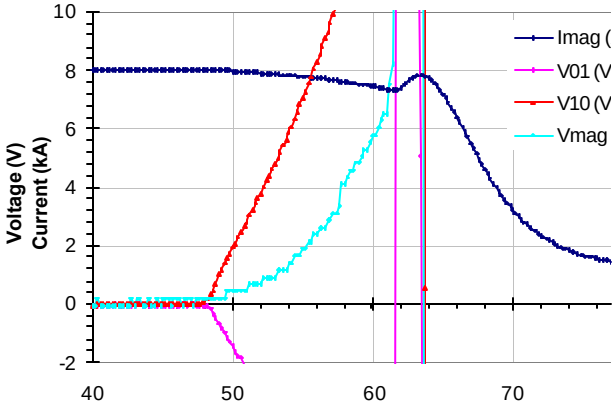

The test continued by repeating the spot heater induced quench at high current, with higher delays (40 and 60 ms). The voltage signals of these events (H03 and H04) show clearly that quench back occurs in SC01, 13-14 ms after the quench start in SC10 (Figure

25). After the quench back, the voltage over the magnet rises faster, inducing a faster current decay. Before the dump activation, the current was ~4 kA in H03.

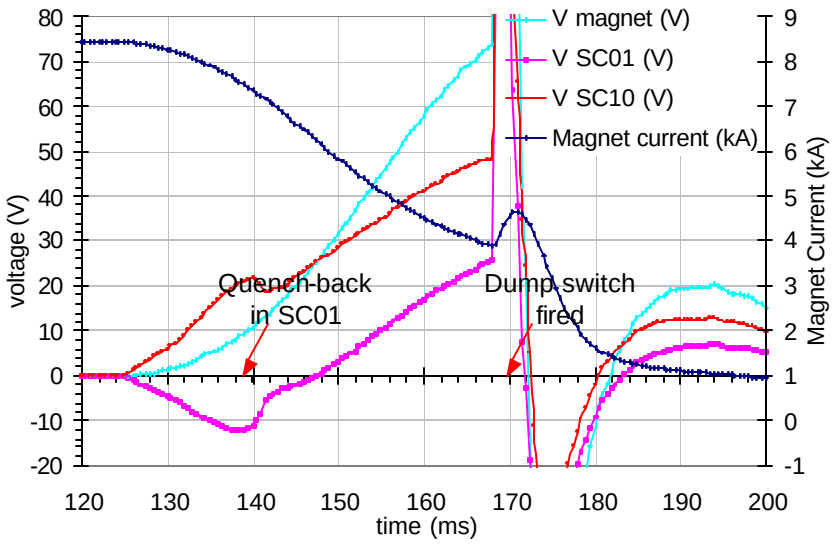

Figure 25: Spot heater event # 3.

To reduce the quench propagation velocity and to avoid quench back, we continued the series of spot heater events lowering the magnet current, and increasing the dump delay times. At 6 kA, the quench back was delayed to 70 ms, and at 5 kA and lower the quench back was not visible. The maximum temperature registered by the Cernox thermometer was ~156 K, during last spot heater event.

After H09, we decided to check the short sample current, by ramping the current to quench at 15 A/s. Unfortunately, the magnet quench prematurely because of the low liquid Helium level in the dewar. In fact, the liquid level in the cryostat was about 60 %, and the leads were cooled only by cold gas. In order to have cooling of the leads a liquid level of 80% is usually necessary. In addition, the temperature sensor shows that the magnet did not recover completely from the previous temperature excursion, because the cooling rate was much slower. The voltage signals of Q10 show that the quench did not start close to the spot heater segment, but most likely started close to the splice of coil 10.

The test series was interrupted at this point because of liquid Helium availability. It was decided to warm up the magnet to room temperature, to perform a thermal cycle, while analyzing the data and planning for another test series with higher peak temperatures.

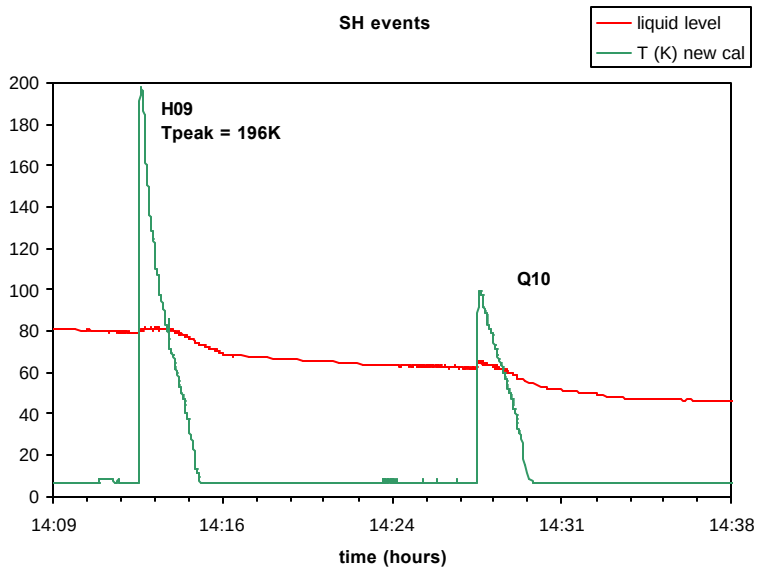

Figure 26: Temperature (K) registered by the Cernox sensor during last spot heater event and the last quench of the first thermal cycle, and the liquid level (%).

4.3.b Data analysis-first thermal cycle

The data analysis consisted in examining the voltage signal of the cable segment close to the spot heater, and the signals coming from the adjacent coil sections. One section included the half turns of the inner layer, from the spot heater to a splice (*V*10*inner*). The other section included the outer layer, and the other half turns of the inner layer, that is from the spot heater to the other joint (*V*10*outer)*.

As an example, we present here in detail the last spot heater event of the first thermal cycle (H09), and the main results of all the other events. Figure 27-left shows the voltage signals and the current decay during H09. The resistance (Figure 27-right) was calculated dividing the voltage by the current (no inductive signal compensation, since the inductance was small).

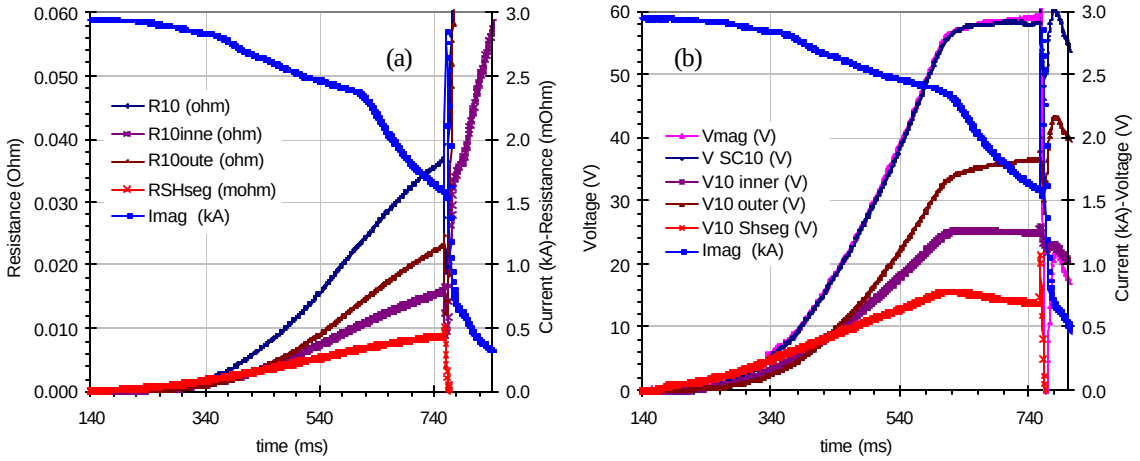

Figure 27: (a) Main voltage and current signals of the last spot heater event of the first thermal cycle; (b) Resistance growth.

From the resistance, we derived the peak temperature by comparison with the resistance measured during the magnet warm up, after the second thermal cycle (see resistance calibration in appendix). We can see in Figure 28 that the peak temperature reached during last event of the first thermal cycle was 340 K.

Table 6 summarizes the thermal shock series in the first thermal cycle. The peak temperature measured via the resistance of the cable (340 K) is much higher than the temperature measured by the sensor during the quench (196 K).

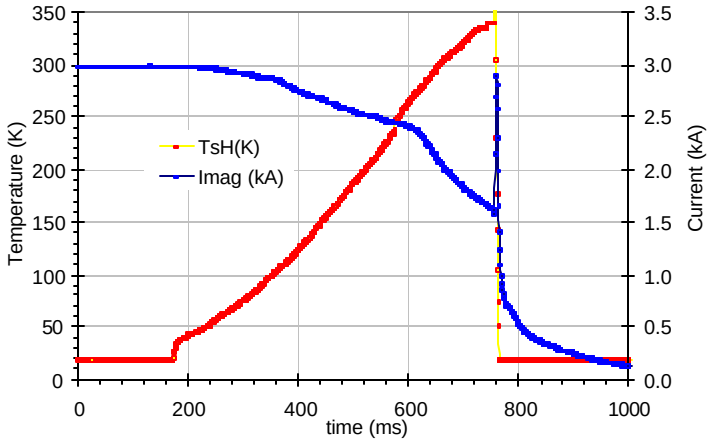

Figure 28: Temperature and current of the last spot heater event of the first thermal cycle.

Ramp #	Current (kA)	Dump delay (ms)	Quench back time SC01 (ms)	MIIts ($10^6 A^2 s$)	T sensor (K)	R SHseg (mOhm)	T SHseg (K)
H01	8.0	10	14	1.29	80	0.074	84
H02	8.0	10	14.2	1.31	80	0.074	80
H03	8.4	40	13	2.11	102	0.161	128
H04	8.0	60	16.5	2.31	110	0.191	144
H05	7.0	80	33	2.79	120	0.240	175
H06	6.0	120	69.5	3.63	160	0.385	295
H07	5.0	140	117	3.63	152	0.386	285
H08	4.0	250	284.5	3.87	174	0.427	325
H09	3.0	500	470	4.12	195	0.440	340

Table 6: Spot heater events – I thermal cycle.

4.3.c Second thermal cycle

Before the second thermal cycle, the power supply was slightly modified, by removing capacitors from the circuit, which subtracted current from the magnet after the quench. This modification allowed a constant current for a longer time after the quench, until reaching the power supply limit. At that moment, the current started to decrease rapidly, and then quench back occurred in SC01. The power supply modification therefore helped increasing the temperature more rapidly during the quench.

The first training quench of the second thermal cycle occurred at 8810 A, a current not yet reached during the first thermal cycle. After this quench, we proceeded with the thermal shock test. Table 7 lists the main parameters of the spot heater events.

Ramp #	Current (kA)	Dump (ms)	MIIts ($10^6 A^2 s$)	R_{SHseg} (mOhm)	T_{SHseg} (K)	T sensor (K)
H10	5.0	200	3.7	0.393	292	194
H11	3.0	440	4.0	0.390	290	183
H12	3.0	440	4.0	0.388	289	185
H13	3.0	440	4.0	0.387	288	191
H14	3.0	450	3.7	0.334	249	165
H15	3.0	450	3.9	0.365	271	193
H17	3.0	514	4.1	0.401	299	198
H18	3.0	800	4.7	0.50	371	245
H19	3.0	1148	5.0	0.56	420	286
H20	3.0	1600	5.4	0.61	451	311
H21	3.0	2000	5.6	0.67	496	337
H22	3.0	2500	5.8	0.70	518	349
H23	3.0	3500	6.1	0.78	579	422

Table 7: Spot heater events – II thermal cycle.

The thermal shock test events of the second thermal cycle are summarized in Figure 29. Each event is represented by a quench number (numbers continued from the first thermal cycle) and a quench current (primary axis on the left), or a peak temperature (secondary axis on the right). The quench current points (diamonds and squares) represent the case of *ramp-to-quench* events, performed in order to check the short sample limit, and therefore to assess the magnet performance. The peak temperature points (triangles) represent the case of *thermal shock* events. The quench current points are represented by squares in the case the quench started within, or at, the voltage taps close to the spot heater; by diamonds, in the case the quench did not start in the spot heater segment. In this case, the quench usually propagated to the spot heater segment after a few ms. The quench is therefore believed to be related to normal magnet training.

During the first thermal shock event at 5000 A, the peak temperature reached about 300 K, even with a dump delay of 200 ms (60 ms more than the previous event at the same current). Not yet understanding the problem limiting the temperature rise, a second heater induced quench was performed at 3000 A, which resulted in the same peak temperature. After few other events at the same current, the cause limiting the experiment was discovered and resolved. The protection system had a limit to the voltage over the leads, which activated the dump switch before the set delay time.

The experiment continued thereafter repeating spot heater induced quenches at 3000 A, with increasing delay times. After reaching a peak temperature of 370 K, the short sample current was checked by ramping up the current to quench. The magnet reached 9028 A, not showing any sign of degradation. The quench started close to the spot heater; in fact, both the spot heater segment and the outer coil signals started at the same time, while the first coil signal had a very short delay of 0.4 ms.

During the following spot heater event, the magnet peak temperature reached 420 K. The following quench current was at the same level as the previous quench. The quench seemed to start close to the spot heater, with all three signals rising at the same time.

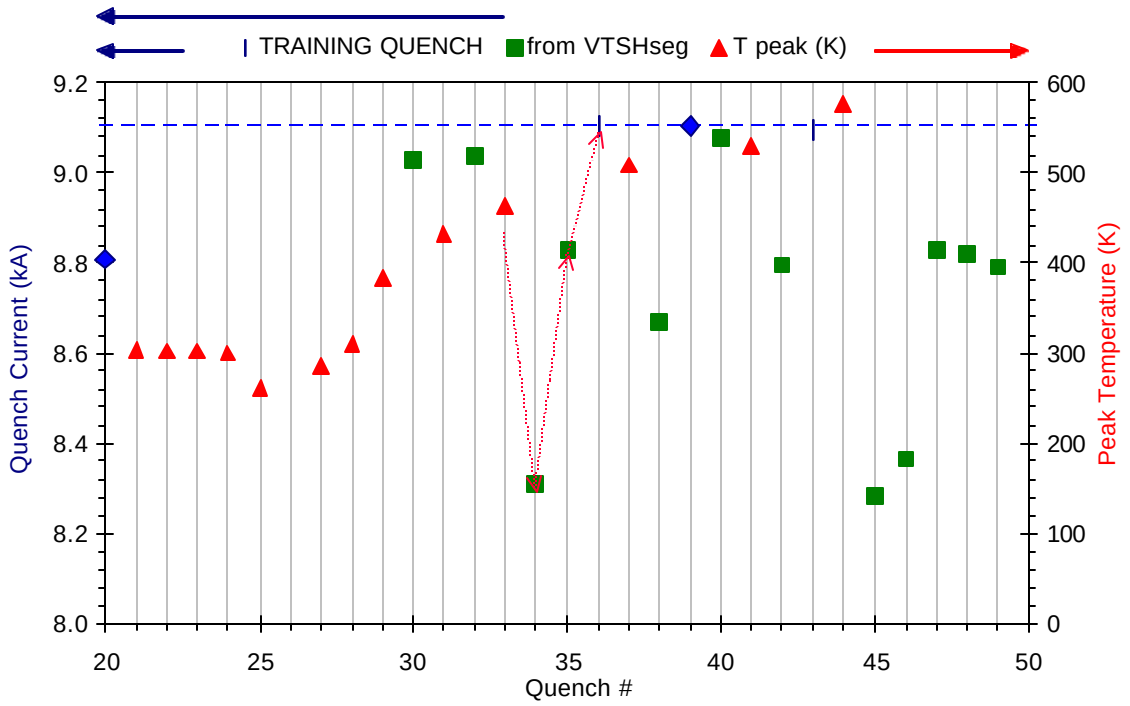

Figure 29: Thermal shock tests during the second thermal cycle: quench current for performance check tests (referred to the left axis) and peak temperatures during quenches for thermal shock tests (referred to the right axis). Arrows highlight the first occurrence of de-training and re-training.

During the next spot heater event, the magnet peak temperature reached 450 K, and the following quench current was 8311 A, 700 A below the previous quench current (8% current decrease). The voltage signals again indicate that the quench started close to the spot heater, with all three signals rising at the same time. During the following current ramp, the magnet quenched at 8830 A, beginning from the spot heater region. The following quench occurred at 9100 A, the maximum current reached by the magnet. The quench did not start within the spot heater segment, where the voltage signal began rising 4 ms after the signals from the other two sections of the coil.

The following spot heater event, lasting two seconds, brought the temperature up to ~500 K. During the next current ramp, the magnet quenched at 8670 A, 4.3 % less than the previous quench current. The quench started simultaneously in all three sections of the coil, including the spot heater segment. The following quench occurred at the maximum current of 9101 A. The quench did not start within the spot heater segment, where the voltage began rising 4 ms after the voltage of the other two sections of the coil. During the next current ramp, the magnet quenched at 9077 A, just below the maximum current. The quench started close to the spot heater, very close to the outer section (reached in 0.4 ms), and then propagated to the inner section (in 1 ms).

The following spot heater event, lasting two and half seconds, brought the temperature up to ~520 K. The following quench occurred at a current of 8796 A (3.4 % less than the maximum). The quench signals started simultaneously in all the three coil sections. The following magnet quench occurred at 9094 A, not within the spot heater segment, where the voltage started rising 4 ms after the voltage of the other two coil sections, as in the previous cases at this current level.

During the final spot heater event (Figure 30), after a delay of three and a half seconds, the temperature reached ~580 K. The following five quenches all occurred below the maximum current and started close to the spot heater together with the signals from the other coil sections. The quenches occurred at 8287 A (8.9 % less than the maximum), then at 8364 A, then at 8830 A (3 %), and finally, decreasing a small percentage, at 8791 A (3.4 % below the maximum current). This was the last quench of the second thermal cycle.

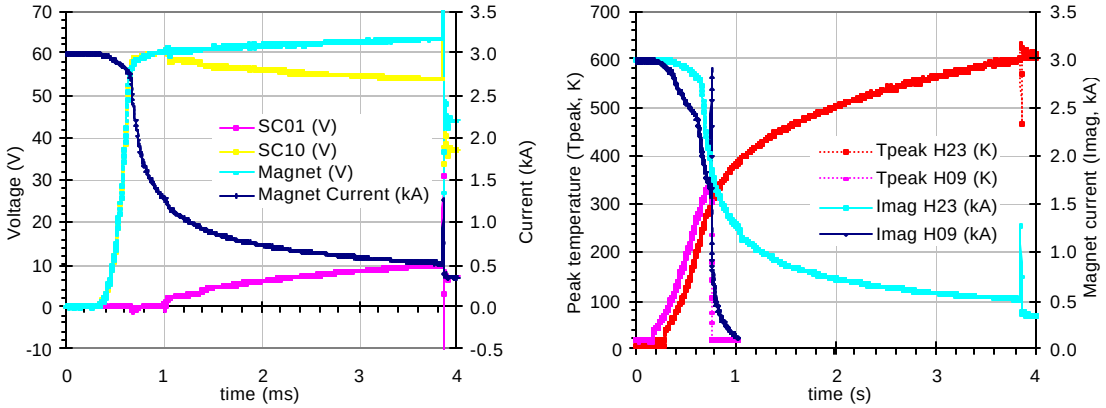

Figure 30: Last spot heater event signals (left) and peak temperature (right); also shown the comparison with H09, last spot heater event of thermal cycle I.

4.3.d Summary of the thermal shock test results

A sub-scaled magnet was built and instrumented to measure the effect of the thermo-mechanical shock during magnet quenches. During the test, the magnet reached the short sample current at 9100 A, corresponding to ~10.5 T. By choice of the delay time of the dump switch, higher and higher temperatures were reached during each quench. After each high temperature excursion, a quench current measurement allowed assessing the magnet performance.

Temperature excursions up to 420 K did not diminish the magnet quench performance. Only after temperature excursions up to 450 K, did the magnet show detraining effects, which occasionally reduced the quench current by about 8 %. Signs of irreversible degradation (a reduction in the maximum current by about 3 %) appeared after temperature excursions up to 580 K.

A more detailed analysis of the quench and the mechanical analysis are in progress, and will be reported in the future.

Acknowledgements

The authors thank the technical group for the great care in the magnet fabrication and the availability during the magnet test.
Thanks to Mark Nyman for the help provided for the set up of the power supply and of the electrical system of the test facility.

Appendixes

I. Cable log sheet

MFG. 9/14/01
OPERATOR: H. Higley & E. Palmerton

CABLE LOG SHEET
LBNL-SUPERCON-AFRD
SUPERCONDUCTING MAGNET CABLES
BLD 52

SAF 7
SC04

Objective : Mfg Baseline #3 Cable, All Superconductor, (Nb3Sn)

- STRAND INFORMATION -

MANUFACTURER :	Oxford		
BILLET #:	Ore-163-B See "stmpS3-O-00817_ORE163-B.xls"		
COMPOSITION :	Nb3Sn		
STRAND Dia.. NOMINAL :	.7mm	INSP. DIA. :	0.70115 mm average.
Cu/SC RATIO NOMINAL :	2.5 Cu / 1 SC	INSP. RATIO :	
FILAMENT TWIST/LENGTH :		DIRECTION :	
SHARP BEND TEST :			
LENGTH PER SPOOL :	64m see respool notes. (stmpS3-O-00817_ORE163-B.xls)		

NOTES:

- CABLING SPECIFICATIONS -

TYPE or SPEC.:	Baseline #3 Cabletype #3				
No. of STRANDS:	20				
PITCH DIRECTION:	Left	PITCH LENGTH:	~~54.88mm~~ 50.80mm		
PLANETARY RATIO:	-0.54:1				
ROLLER ID #:	P17 & P18	WIDTH:	7.928/7.922	ANGLE:	Nom- 0
MANDREL ID #:	4	WIDTH:	6.72 mm	THICKNESS:	.41 mm "Thin?" H.H.
LUBRICATION :	100% 4-BR nominally 1 drop/pitch				
STRAND TENSION:	2.2 kg +/- .05	TURKS HEAD LOAD "SGM":		44.0 kg +/-2	
Nom. THICKNESS:	1.275mm				
Nom. WIDTH:	7.9mm				
Nom. ANGLE:	0				

- FINISHED CABLE -

SC-04 Action 1 May

	S-3-O-00817	
FINISHED LENGTH:	56m	2 9 m
Avg. THICKNESS:		
Avg. WIDTH:		
Avg. ANGLE:		
Cable/Strand Yield:		

RESIDUAL TWIST/Mtr.: Less than 90 deg./m at tail end.
ETCH for FILAMENT DAMAGE:

NOTES : Had some difficulty with gaps between strands. We determined that this was due to reduced strand diameter. Earlier cables used .711mm strand this cable is .701mm.
We decided to reduced the pitch length to compensate. The first 3m at the point end of this cable are at the longer 54.8mm pitch length. The 2m sample given for 10stack came from the tail end of this run. Also see photographs of MgO paper core test. MgO-Paper-Core-Test-S3O-00817.JPG

"Note. The first nine meters have some variability. This will be designated as the point end. We will insulate the cable and leave the Point end at the hub un-insulated.
Values reported here as average are only for the final 45.3 m of cable on the spool."

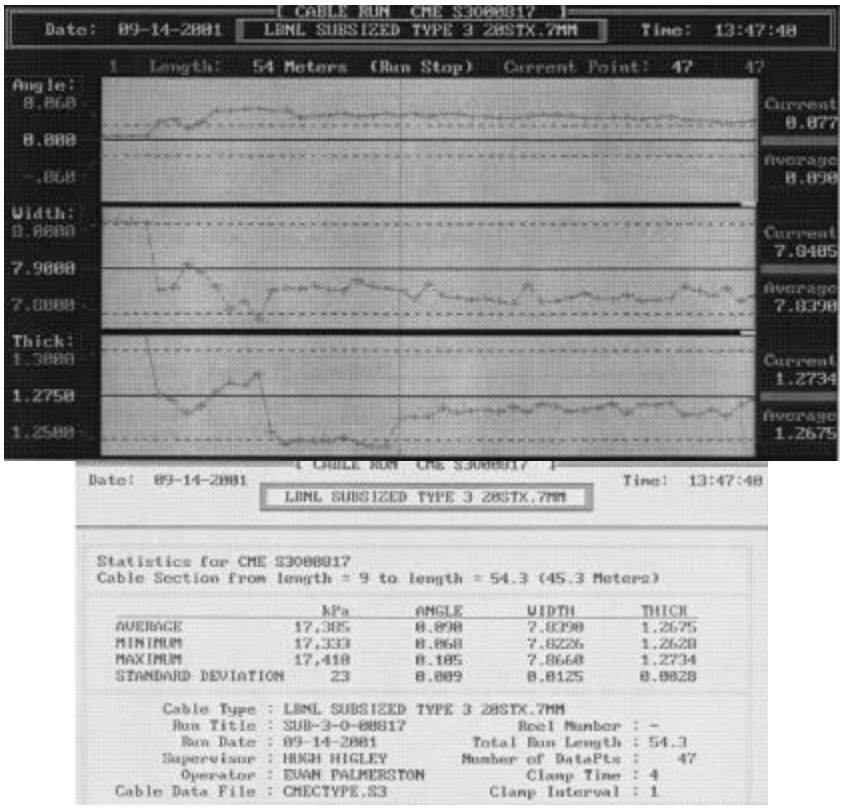

Comment: After SC04 30 m were left. SC10 used about 22 m. Therefore, most of the 9 m cable segment at the "point end" was probably not included in the coil.

II Temperature calibration during warm up

In order to estimate the peak temperature reached by the segment of magnet underneath the spot heater, the magnet was instrumented with two voltage taps that enclose the position of the spot heater and read the voltage across a 89 mm segment of cable. In order to have a reliable and accurate estimate of the temperature of the segment, we found it was necessary to perform a calibration of the resistance of the segment, as a function of temperature. Therefore, during the magnet warm-up, the resistance of the spot heater segment was recorded, together with the temperature at different locations. In addition, the magnet was heated up to 330 K, in order to determine the linear dependence of the resistance at room temperature, and to extrapolate the resistance at higher temperatures. The magnet was heated by applying a current through the coils and by an external heater placed in the bottom of the cryostat. To warm up the magnet faster, a DC current of 10 A was applied to the magnet, while the bottom heater was set to its highest power setting (50 V, 2 A). This brought the temperature from 150 K up to 330 K. When the temperature reached 330 K, the magnet current was reduced to 0.5 A, and the resistor was switched off. Figure 31 shows the temperature, as a function of time, recorded by the two platinum temperature sensors and by the CERNOX close to the spot heater in coil 10 (TSC10). The two platinum sensors are attached to the magnet shell. One sensor is close to the lead end of the magnet (Ttop15), and the other is close to the return end (Tbot15).

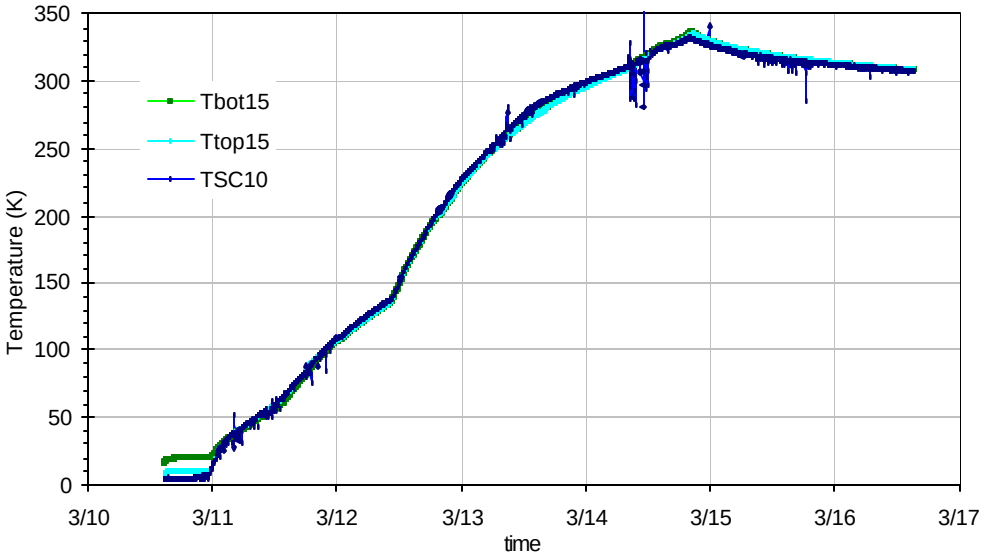

Figure 31: temperature sensor data during warm up.

Above the initial transition phase, the temperatures registered by these thermometers are close to each other, indicating that the warm-up procedure was slow enough for a uniform temperature distribution over the entire magnet. The Cernox sensor was not accurately calibrated before, while the two platinum sensors had already been calibrated in the past. Therefore, the Cernox sensor was calibrated over the Ttop15 sensor, in order to get a better estimate of the temperature. Figure 32 shows the resistance as a function of temperature recorded by the top platinum temperature sensor.

Since the recovering curve to room temperature was slightly different from the warm up, a second warm up to 330 K was performed with I_{mag} = 0.5 A and maximum power in the resistor, on order to find the source of the discrepancy.

There are three sources of heat inside the cryostat during the operation:

1. **Temperature sensor**: when the power in the sensor it is too high its cooling capacity can be impaired, and the sensor can read a higher temperature than the actual temperature. This effect should be negligible because the temperature sensor is read with a four-wire system minimizing the power inside the sensor during the time of the reading.
2. **Magnet**: if the power in the magnet is too high with respect to its cooling capacity the temperature of the magnet is higher than the temperature at the platinum sensors locations (temperature sensor lags behind in responding). With 10 A in the magnet, and a resistance per length of ~4.5 mOhm/m, there is a heat source of 45 mW/m in the coil.
3. **Heater**: if the power in the resistor is too high with respect to the heat capacity of the magnet, the reading of the resistance of the magnet could lag behind the temperature of the environment.

To better estimate the effect of the resistor compared to the effect of the heat developed by the coil, the resistor was turned ON, to its maximum power, and the current at left 0.5 A. It was concluded that the effect of the resistor is negligible compared to the effect of the heat generated by the current in the magnet. The warm up curve with the

resistor ON, and I_{mag} = 0.5 A, was within the error of the measurements of the cooling down curve (resistor OFF, I_{mag} = 0.5 A).

Secondly, the error in the voltage readings was checked. A small the offset in the voltmeter reading the magnet voltage was measured. This offset affects more the measurements at low currents, while it is negligible at 10 A. It was then concluded that the first calibration curve was correct.

Figure 32 shows the comparison of the resistance measured as described above, and data from literature. The resistance has been calculated from resistivity values, and geometrical factors, including the Copper content of 62.5 %, the transposition pitch of 17 degrees, and a length between the voltage taps of 93 mm, which corresponds to the distance edge-to-edge. We can notice that the measured resistance is slightly higher than the value expected for oxygen free high conductivity Copper (OFHC [11]) at 293 K (ρ_{Cu}=1.69· 10^{-8} Ω· m) of about 10%, and about 4% with respect of data from measurement of NbTi strands [12] (ρ_{Cu}=1.8· 10^{-8} Ω· m). The parameterization of the Copper resistivity from NIST [13], gives a room temperature value of ρ_{Cu}=1.76· 10^{-8} Ω· m.

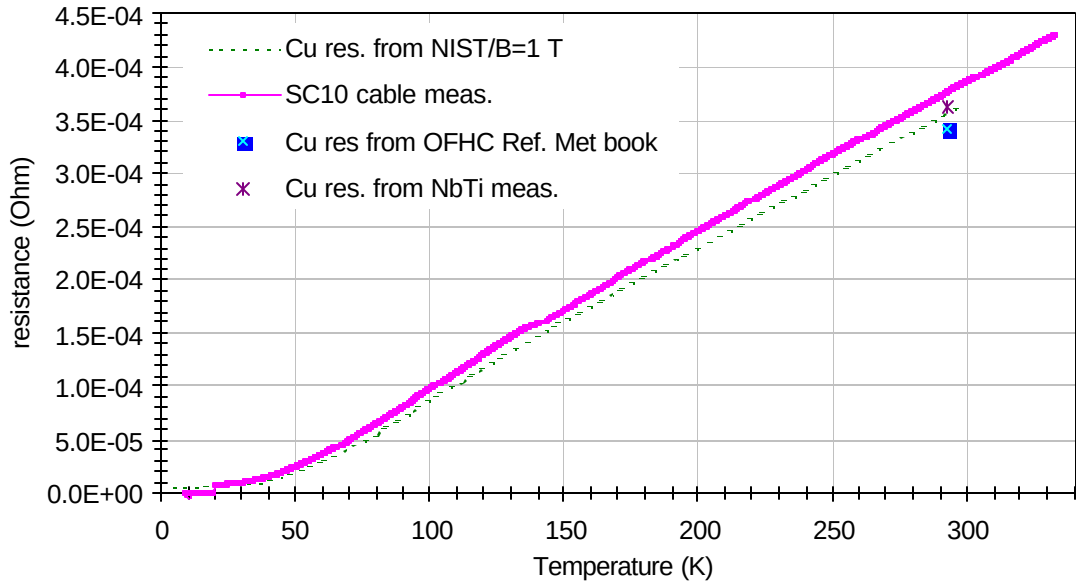

Figure 32: Resistance of the cable segment beneath the spot heater vs. temperature: comparison of measurement and data from literature.

Figure 33 shows the extrapolation of the data measured in SC10, and the comparison with data of HFHC Copper. The difference in resistance between the two curves remains within 10%, up to 600 K. The difference in temperature remains is also about 10 %.
The linear function used to approximate the data is

$$T = (R[\text{ohm}]+1.96\cdot 10^{-5})/1.35\cdot 10^{-6} \quad [\text{K}].$$

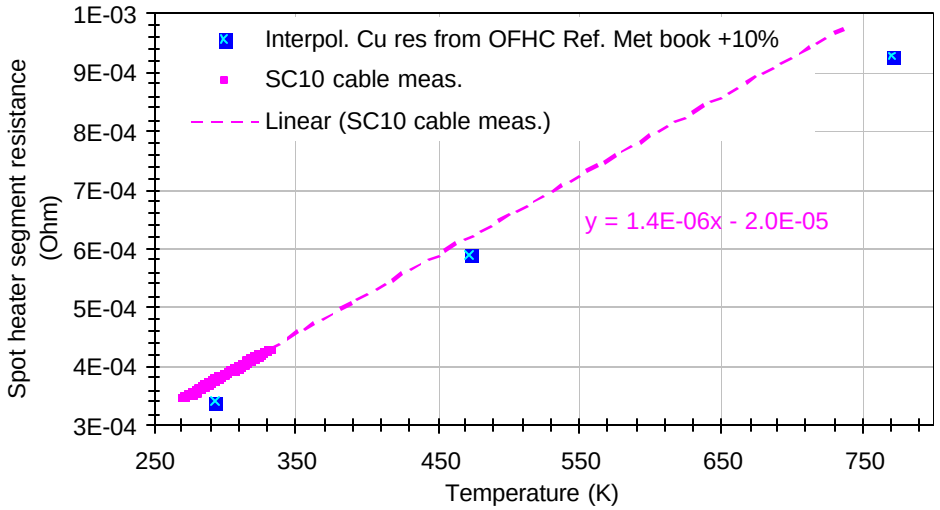

Figure 33: Resistance of the cable segment close to the spot heater vs. temperature: comparison of measurement and data from literature.

References

[1] L. Imbasciati et al., "Quench Protection of High Field Nb_3Sn Magnets For VLHC," proceedings of PAC, June 2001

[2] L. Imbasciati et al., "Quench-Tests on Nb_3Sn Cables - Run 1," Fermilab Technical Division note, TD-01-075, November 2001

[3] L. Imbasciati et al., "Effect of Thermo-Mechanical Stress during Quench on Nb_3Sn Cable Performance," *IEEE Trans. Appl. Supercond*., June 2003, ASC 2002

[4] R.R. Hafalia et al., "An Approach for Faster High Field Magnet Technology Development," *IEEE Trans. Appl. Supercond*., June 2003, proceedings of ASC02

[5] R.R. Hafalia et al., "A new Support Structure for High Field Magnets," SC-MAG 738, Lawrence Berkeley National Laboratory, Sept. 2001 (MT-17)

[6] S. Caspi et al., "The Use of Pressurized Bladders for Stress Control of Superconducting Magnets," *IEEE Trans. App. Supercond.*, vol. 11 No. 1, p. 2272, March 2001

[7] M. Coccoli, "Fabrication and Testing of Superconducting Cables and Subscale Magnets for a More Effective Approach to Future Accelerators R&D and Fabrication," *Laurea thesis*, University of Milan, Italy, April 2003

[8] M. Coccoli, L. Chiesa, "SM01a and SM01b Test Results," internal note, LBNL-50145 SC-MAG 775, Feb. '02

[9] Private communication

[10] L. Chiesa et al., "Performance Comparison of Nb_3Sn Magnets at LBNL," *IEEE Trans. Appl. Supercond*., June 2003, proceedings of ASC02

[11] Smithells Metals Reference Book, 7th edition, Brandes and Brook

[12] S.S. Kozub, Y.V. Shpakovich, A.V. Zlobin, "Thermal Conductivity and Electric Resistance of Composite Wires," Cryogenics, V. 32, ICEC supplement, p. 295-299

[13] N.J. Simon, E.S. Drexler, R.P. Reed, "Properties of Copper and Copper Alloys at Cryogenics Temperatures," NIST Monograph 77